CORRELATION BETWEEN MICROSTRUCTURAL CHARACTERISTICS AND SPECIMEN-LEVEL SHRINKAGE OF ALKALI-ACTIVATED BINDER CONCRETE

Anju H Alex [1], Kruthi K Ramagiri[1], ArkamitraKar[1]

1. Birla Institute of Technology and Science (BITS)-Pilani, Hyderabad Campus, Telangana, India

ABSTRACT. Alkali-activated binders (AAB) are produced by the reaction of an alkaline solution with aluminosilicate rich industrial by-products such as fly ash or slag. Apart from low CO_2 emissions, AAB concrete possesses mechanical properties similar to and in certain cases better than those of portland cement (PC). However, its commercial viability can be improved only through further investigation into its durability parameters. Shrinkage is one such critical parameter which affects the durability of concrete. Limited studies reported on the shrinkage strains of AAB systems focused mainly on hardened AAB pastes and mortars. Very few studies are conducted on AAB concrete specimens and no models are reported to predict the shrinkage strains of AAB concrete. However, the unavailability of adequate data impedes the practical application of AAB concrete on a large-scale. Hence the present study aims to evaluate the shrinkage behaviour of AAB concrete and formulate a model to correlate it with the observed microstructural characteristics. The shrinkage strains are measured for two different mixes with fly ash: slag ratio of 70:30 (FS 30) and 50:50 (FS 50) under ambient curing conditions. Microstructural characteristics are studied using scanning electron microscopy and energy dispersive spectroscopy (SEM/EDS) analysis. The compressive strength of FS 50 is 28.6% higher and shrinkage strain at 180 days is 0.4% higher than FS 30. FS 30 exhibits lower shrinkage, provides an optimal combination from the workability and economy aspects and can be recommended for practical use based on the requirement of user.

Keywords: Durability, Alkali-activated binders, Shrinkage.

Anju H Alex is a Master's Degree student in Civil Engineering at BITS-Pilani, Hyderabad Campus, India. Her research interest includes concrete shrinkage characteristics.

Kruthi K Ramagiri is pursuing her PhD in Civil Engineering at BITS-Pilani, Hyderabad Campus, India. Her topic of research is the service life performance of concrete specimens with alkali-activated binders.

Dr Arkamitra Kar is an Assistant Professor of Civil Engineering at BITS-Pilani, Hyderabad Campus, India. His research interests are the chemistry of advanced construction materials and the reuse of waste materials to encourage sustainable construction practices.

INTRODUCTION

Portland cement (PC) production is considered to be one of the major contributors to global warming as 1 ton of CO_2 is emitted for each ton of PC produced. Apart from being a highly energy-consuming process, the manufacture of PC also accounts for approximately 5-7% of the global CO_2 emissions [1-2]. With increasing need and demand for sustainable construction practices, low carbon-emission binders have to be adopted as alternatives to PC. Alkali-activated binders (AABs) can act as a suitable option, provided they meet the necessary engineering and durability criteria. AABs are produced by the reaction of an alumino-silicate precursor, generally industrial by-products such as fly ash and/or slag, with an alkaline solution composed of sodium or potassium hydroxides and/or silicates. AAB concrete exhibits engineering properties comparable to, or in some cases, superior to PC [1-8]. However, the commercial viability of AABs can be improved only with further investigation of its long-term durability properties.

Shrinkage is one of the most critical properties affecting the durability of concrete. Under restrained conditions, shrinkage in concrete leads to cracking and subsequent ingress of moisture and other harmful chemicals. This leads to a further decrease in the durability of concrete. Existing research reported on the shrinkage of AAB focused mainly on hardened AAB pastes and mortars [3, 9-19]. Limited information is available regarding the shrinkage strains of AAB concrete. Available research [20] shows that drying shrinkage strains are compared with the values predicted by an existing model [21] for inclusion in the Australian Standard for Concrete Structures AS3600 [22]. However, that equation and that standard code of practice are valid only for PC concrete and it resembles the rectangular hyperbolic form suggested by ACI Committee 209R-92 [23] to predict shrinkage strains of PC concrete, although the coefficients are slightly different in the equations proposed by the existing model [21]. The measured drying shrinkage strains of heat-cured fly ash-based AAB concrete specimens are significantly smaller than the predicted values. On the other hand, for the specimens cured in ambient conditions, the drying shrinkage strains are significantly larger than the predicted values [13, 20]. One potential way to reduce the drying shrinkage for AAB concrete is a partial replacement of fly ash with slag. Previous research investigated the effects of blending of ground granulated blast furnace slag with fly ash on the strength development and drying shrinkage up to a period of 180 days for concrete with AAB [24]. The results concluded that shrinkage decreased with the increase of slag content in AAB concrete cured at room temperature. However, only 10% and 20% mass replacement of fly ash by slag was examined [24] and the results were reported in accordance with the existing Australian standards only. Another study carried on alkali-activated fly ash-slag systems (AAFS) shows that shrinkage increases with slag content and decreasing the Ms modulus (i.e. SiO_2/equivalent Na_2O in the activating solution) [25-26].

Studies on AAB concrete specimens evince the significant influence of the distribution of mesopores and the volume fraction of the hardened paste on its shrinkage strains at specimen level [5, 27-28]. But, no models have been reported till date to predict the shrinkage strains of AAB concrete. Existing conventional models, applicable for PC, are not suitable to predict the shrinkage behaviour of AAB concrete [29]. However, in order to promote practical application of AAB concrete on a large-scale, adequate data on its long-term durability performance is necessary. Hence the present study aims to address the above issues by i) developing AAB concrete mixes using varying proportions of fly ash and slag under ambient curing conditions, ii) evaluating the shrinkage behaviour of these mixes through

laboratory testing, and iii) formulating a model to correlate the shrinkage strains with the corresponding microstructural characteristics. The shrinkage strains are measured for two different AAB concrete mixes with the varied proportion of precursors under ambient curing conditions (31±2°C). Microstructural characteristics are studied using scanning electron microscopy and energy dispersive spectroscopy (SEM/EDS) analysis.

MATERIALS AND METHODS

Materials

Class F fly ash (FA), complying with ASTM C618 (Standard Specification for Coal Fly Ash and Raw or Calcined Natural Pozzolan for Use in Concrete) [30] obtained from National Thermal Power Corporation (NTPC) Ramagundam, from the state of Telangana, India was used. Ground granulated blast furnace slag (slag) conforming to ASTM C989 (Standard Specification for Slag Cement for Use in Concrete and Mortars) [31] used in this study was acquired from JSW Cement limited. For the alkaline activating solution, sodium hydroxide (food grade NaOH pellets with 99% purity) and sodium silicate (industrial grade Na2SiO3 with 29.5% SiO_2 and 14.7% Na_2O by weight) from Hychem Chemicals limited are utilized. Activating solution was prepared a day prior to the usage. Crushed granite aggregate with a nominal maximum size of 10mm and locally available 4.75 mm graded river sand complying with ASTM C33 (Standard Specification for Concrete Aggregates) [32] were used in this study. Commercially available polycarboxylic ether (PCE) based high-range water reducing admixture more commonly, superplasticizer (SP) used in this study was supplied by BASF Chemicals and conforms to ASTM C494 (Specification for Chemical Admixtures for Concrete) [33]. Normal potable (tap) water is used for mixing.

Mix proportions and specimen preparation

Two mixes with varying proportions of precursors (flyash and slag) were designed to examine their effect on shrinkage of AAB concrete. The mix compositions used are presented in Table 1. The water-to-solids ratio for concrete was maintained at 0.3.

Table 1 Details of AAB concrete mix

MATERIALS	FS 30	FS 50
FA/Slag	70/30	50/50
Flyash (kg/m^3)	280	200
Slag (kg/m^3)	120	200
Activator Solution (kg/m^3)	140	140
Coarse Aggregate (kg/m^3)	1209	1209
Fine Aggregate (kg/m^3)	651	651
Water (kg/m^3)	67.65	67.65
SP (l/m^3)	3.14	4

For measuring shrinkage strains of AAB concrete, prism specimens of dimensions 280×25×25 mm were prepared and tested in accordance with specifications of

ASTM C157/157M (Standard Test Method for Length Change of Hardened Hydraulic-Cement Mortar and Concrete) [34]. The dry ingredients were mixed to achieve a uniform blend. Then the addition of activating solution to the mix was followed by the measured quantity of water and SP. The specimens were cured at ambient temperature (31±2ºC). Owing to slow strength gain [35-37], the specimens were cured under sealed conditions for 72 hours instead of 24 hours as specified by ASTM C157 [34].

Methods

Compressive strength test of concrete is performed according to ASTM C39 (Standard Test Method for Compressive Strength of Cylindrical Concrete Specimens) using HEICO compression testing machine (CTM) of 2000 kN capacity.

Drying shrinkage was measured in terms of length change of the specimen with respect to its initial length. Following curing, the initial length of the specimen was measured using a standard length comparator in compliance with ASTM C490 (Standard Practice for Use of Apparatus for the Determination of Length Change of Hardened Cement Paste, Mortar, and Concrete) [38]. The subsequent length measurements were made at regular intervals of 24 hours.

Shrinkage strains were then calculated as the ratio of change in length to the initial length. The length change of the specimen at any age was calculated by the formula, specified by ASTM C157/C 157M [34], as mentioned below

$$\boldsymbol{\Delta L = \frac{CRD - initial\ CRD}{G}}$$

where:
ΔL = length change of specimen at any age,
CRD = difference between the comparator reading of the specimen and the reference bar at any age, and
G = the gauge length [280 mm].

Microstructural characteristics of the samples were studied using scanning electron microscopy (SEM) accompanied by energy dispersive x-ray spectroscopy (EDS). The samples prepared using the same procedure and under identical conditions as the prism specimens were analysed for microstructural characteristics. Prior to SEM analysis, the samples were dehydrated in an environment of 100°C for 2 hours. The samples were then coated with a 10 nm layer of gold-palladium, to make them electrically conductive using Leica EM ACE200 sputter coater. SEM analysis of the samples was performed using FEI Apreo SEM equipped with a secondary electron detector. The micrographs were captured at a magnification of 2500x and an operating voltage of 20 kV. The working distance throughout the analysis was maintained as 10 mm.

EDS analysis of each sample was performed simultaneously after recording the micrograph. From the atomic percentages obtained, the ratios of Ca/Si, Na/Al, and Si/Al were calculated. Each reaction product has a characteristic range for these atomic ratios. The volume fractions of these reaction products were thus estimated based on these ratios as identified from existing literature [39]. By combined analysis of SEM micrographs and EDS results, volume fractions of the reaction products formed were calculated.

RESULTS

The mean compressive strength of three specimens for FS 30 and FS 50 at 28 days is 52.04 and 66.91 MPa respectively. The improved compressive strength with increase in slag content is attributed to the formation of the additional C-S-H matrix [40].

The drying shrinkage of AAB concrete with varied proportions of precursors is plotted in Figure 1.

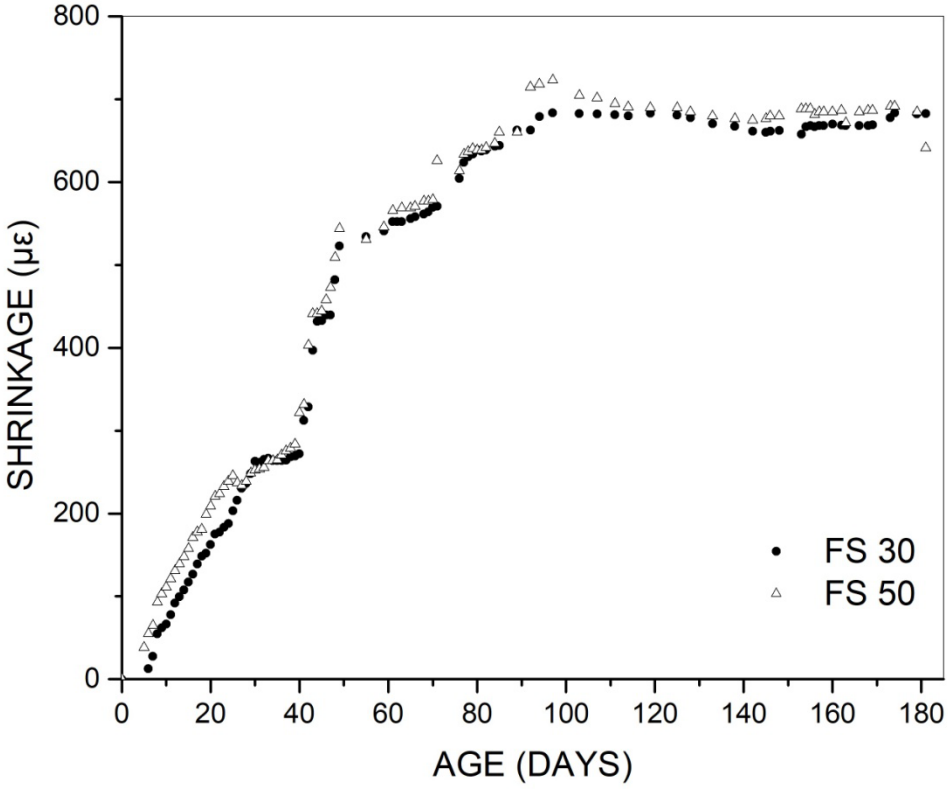

Figure 1 Shrinkage strains of AAB concrete

The maximum shrinkage strain observed in FS 30 and FS 50 AAB concrete, at the age of 180 days, is 682.2 and 684.8 με respectively. Of the various factors affecting shrinkage of AAS and AAFA mixes, it is reported that the governing factors are pore structure and the free water content [42-44]. But studies on AAB with FA and slag show that the shrinkage behaviour is highly influenced by its microstructure [41]. AAB concrete with FA and slag has a complex microstructure with both N-A-S-H matrix, characteristic of low-Ca systems and C-S-H matrix, characteristic of high-Ca systems [45-50].

The reaction products N-A-S-H and C-S-H coexist and cannot be distinguished from the SEM micrographs. Therefore, the fraction of reaction products formed was determined by EDS analysis and the results are presented in Table 2.

Table 2 Fraction of reaction products formed at different ages

AGE OF THE SPECIMEN (DAYS)	FRACTION OF REACTION PRODUCTS FORMED (%)	
	FS 30	FS 50
1	5.55	5.55
3	11.76	16.67
7	16.67	27.78
28	33.33	27.78
90	28.57	23.89

With the incorporation of slag, the fraction of reaction products increased at early ages. Previous research shows that shrinkage of AAB increases with slag content [51, 52] and a similar trend is observed in the present study. Increase in the proportion of slag accelerates the polymerization reaction, as evident from the EDS results [Table 2]. This result in greater volume reduction of reaction products as compared to the volume occupied by the original binder, thereby increasing shrinkage. SEM micrographs of FS 30 and FS 50, for different ages, are presented in the figures below.

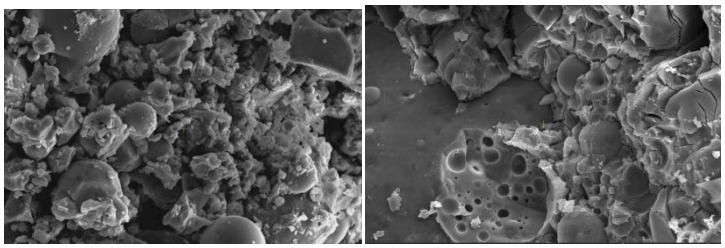

a. FS30 b. FS50

Figure 2 SEM micrographs of AAB concrete at 1 day

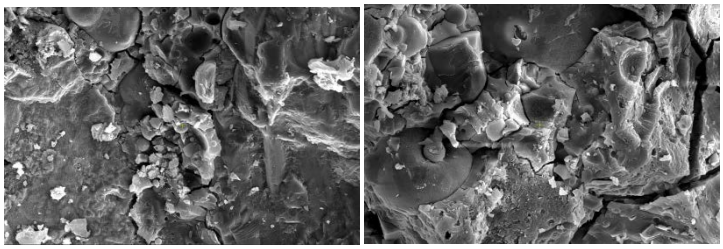

a. FS30 b. FS50

Figure 3 SEM micrographs of AAB concrete at 3 days

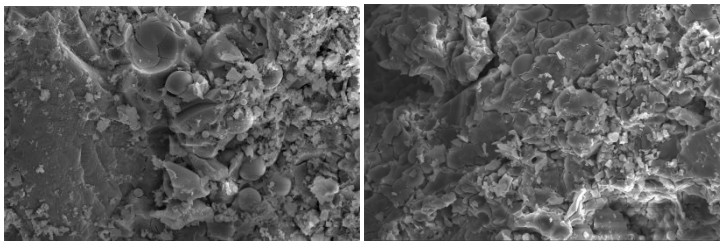

a. FS30 b. FS50

Figure 4 SEM micrographs of AAB concrete at 7 days

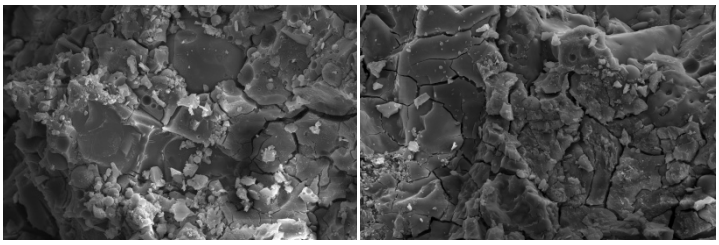

a. FS30 b. FS50

Figure 5 SEM micrographs of AAB concrete at 28 days

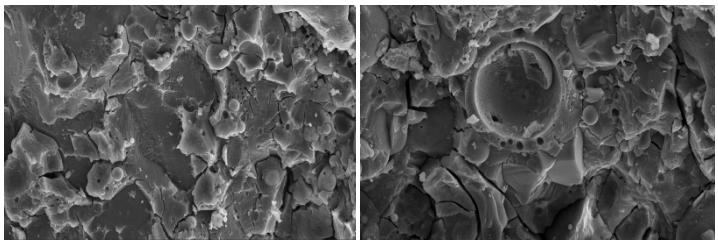

b. FS30 c. FS50

Figure 6 SEM micrographs of AAB concrete at 90 days

SEM micrographs show different morphologies of AAB concrete with varying proportion of precursors. Early age micrographs show unreacted fly ash and slag particles embedded in the matrix. FS 50 forms a binding phase at early ages, owing to the rapid reaction. With the increase in age of samples, less unreacted particles were observed. Micrographs of both FS 30 and FS 50 show denser and compact microstructure at 90 days compared to early ages. The shrinkage of FS 50 is only marginally greater than FS 30, with strains in a similar range.

From SEM and EDS analysis, it is evident that with time there is an increase in the fraction of reaction products [Table 2 and Figures 2-6]. This results in decreased porosity and pore connectivity of AAB concrete [53-55]. This improves the volumetric stability of concrete [56], thereby reducing the rate of shrinkage at later ages. In the present study, the shrinkage rate of FS 30 and FS 50 reduced after 90 days.

The model for prediction of shrinkage strains of AAB concrete, with varying proportions of precursors, was developed such that it fits the available experimental data. The general form of the equation for predicting shrinkage given by ACI 209R-92 [23] is

$$\boldsymbol{\varepsilon(t) = \frac{Kt^n}{A + Bt}} \tag{1}$$

Using the above equation, the proposed model for regression analysis is

$$\boldsymbol{f(x) = \frac{ax^d}{b + cx}} \tag{2}$$

Equation 2 was given as a custom equation in the curve fitting toolbox of MATLAB and the best curve fit is found. The values of a, b, c, d, and root-mean-square error (RMSE) for all the mixes are presented in table 3.

Table 3 Output for the proposed model from MATLAB

MIX	A	b	c	d	RMSE
FS 30	1.862e-04	2.183e-05	1.869e-06	1.41	73.87
FS 50	1.091e-04	9.883e-06	9.38e-07	1.38	70.68

The comparison of experimental data to model prediction is presented in figure 7.

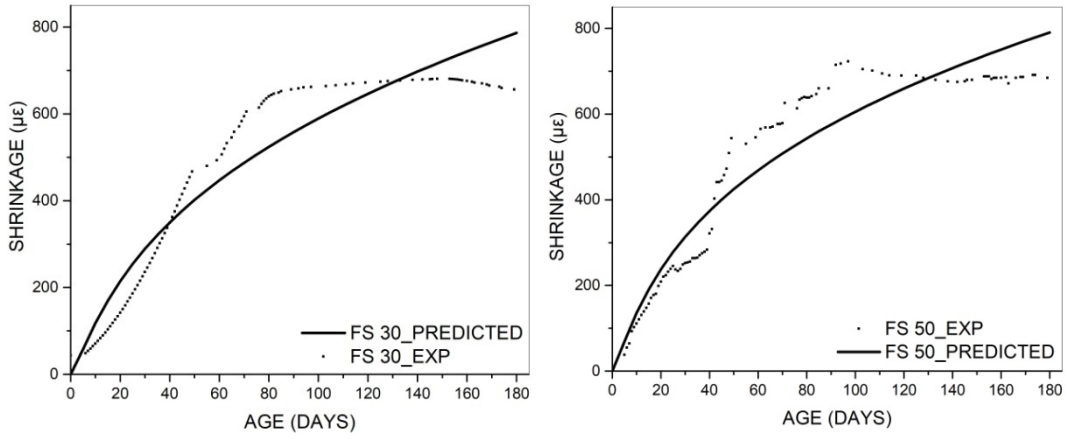

a b

Figure 7 Experimental Vs predicted shrinkage

The proposed model adequately predicts the shrinkage of FS 30 and FS 50 mixes, as presented in Figure 7. For both FS 30 and FS 50 mixes, the predicted line is observed to follow the trend of experimental data [Figure 7].

CONCLUDING REMARKS

In this paper, the shrinkage of two AAB concrete mixes with the varied proportion of precursors is examined. Their shrinkage behaviour is correlated with the microstructural characteristics examined using SEM and EDS analysis. A model has been formulated to predict the shrinkage of AAB concrete. From the outcomes of the present study obtained, the following conclusions are made:

- Greater slag content in the mix increased the shrinkage strains, with FS 50 exhibiting higher shrinkage. The shrinkage strain observed in FS 30 and FS 50 AAB concrete, at 180 days, is 682.2 and 684.8 με respectively.
- Incorporation of more slag accelerated the polymerization reaction resulting in greater volume reduction of the reaction products as corroborated by SEM and EDS analysis.
- With time, the volumetric stability of AAB concrete improved due to an increase in the fraction of reaction products formed. This resulted in a decrease in the rate of shrinkage of FS 30 and FS 50 after 90 days.
- The experimental data of both FS 30 and FS 50 follows the predicted shrinkage model based on ACI 209:2R-92.

- Several variations of AAB precursor ratios are required to develop more generalized prediction equations for shrinkage of concrete with AAB. If heat-cured AAB is considered, a factor for that should also be incorporated into the model. Finally, strain data can be collected over a period of 365 days to observe a more comprehensive variation of the shrinkage strains of concrete with AAB.

The results from the present study suggest that the microstructural analysis function as an effective tool to understand the specimen-level properties of concrete. With the varying proportion of precursors and the age of concrete, the changes in the microstructure of AAB concrete correlates well with its observed shrinkage trend.

REFERENCES

1. RASHAD A M, Properties of alkali-activated fly ash concrete blended with slag, *Iranian Journal* of Materials Science and Engineering, 2013, Vol. 10, No. 1, pp 57-64.
2. NATH P AND SARKER P K, Effect of GGBFS on setting, workability and early strength properties of fly ash geopolymer concrete cured in ambient condition, Construction and Building Materials, 2014, Vol. 66, pp.163-171.
3. LEE N K AND LEE H K, Setting and mechanical properties of alkali-activated fly ash/slag concrete manufactured at room temperature, Construction and Building Materials, 2013, Vol. 47, pp 1201-1209.
4. SOFI M, VAN DEVENTER J S J, MENDIS P A AND LUKEY G C, Engineering properties of inorganic polymer concretes (IPCs), Cement and Concrete Research, 2007, Vol. 37, No. 2, pp.251-257.
5. COLLINS F G AND SANJAYAN J G, Workability and mechanical properties of alkali activated slag concrete, Cement and Concrete Research, 1999, Vol. 29, No. 3, pp 455-458.
6. BAKHAREV T, SANJAYAN J G AND CHENG Y B, Effect of admixtures on properties of alkali-activated slag concrete, Cement and Concrete Research, 2000, Vol. 30, No. 9, pp 1367-1374.
7. FERNÁNDEZ-JIMÉNEZ A, PALOMO J G AND PUERTAS F, Alkali-activated slag mortars: mechanical strength behaviour, Cement and Concrete Research, 1999, Vol. 29, No. 8, pp.1313-1321.
8. FERNÁNDEZ-JIMENEZ A M, PALOMO A AND LOPEZ-HOMBRADOS C, Engineering properties of alkali-activated fly ash concrete, ACI Materials Journal, 2006, Vol. 103, No. 2, pp 106.
9. MA Y, YE G, The shrinkage of alkali activated fly ash, Cement and Concrete Research, 2015, Vol. 68, pp 75-82.
10. THOMAS J J, ALLENA J, JENNINGS H M, Density and water content of nano-scale solid C-S-H formed in alkali-activated slag (AAS) paste and implications for chemical shrinkage, Cement and Concrete Research, 2012, Vol. 42, No. 2, pp 377-383.

11. JIA Z, YANG Y, YANG L, ZHANG Y, AND SUN Z, Hydration products, internal relative humidity and drying shrinkage of alkali activated slag mortar with expansion agents, Construction and Building Materials, 2018, Vol. 158, pp 198-207.
12. YE H AND RADLIŃSKA A, Shrinkage mechanisms of alkali-activated slag, Cement and Concrete Research, 2016, Vol. 88, pp 126-135.
13. COLLINS F, SANJAYAN J G, Strength and shrinkage properties of alkali-activated slag concrete placed into a large column, Cement and Concrete Research, 1999, Vol. 29, No. 5, pp 659-666.
14. CARTWRIGHT C, RAJABIPOUR F AND RADLIŃSKA A, Shrinkage characteristics of alkali-activated slag cements, Journal of materials in civil engineering, 2015, Vol. 27, No. 7, B4014007.
15. HANSEN T C, Drying shrinkage of concrete due to capillary action, Matériaux et Construction, 1969, Vol. 2, No. 1, pp 7-9.
16. ALY T AND SANJAYAN J G, Mechanism of early age shrinkage of concretes, Materials and structures, 2009, Vol. 42, No. 4, pp 461.
17. SHI C, Strength, pore structure and permeability of alkali-activated slag mortars, Cement and Concrete Research, 1996, Vol. 26, No. 12, pp 1789-1799.
18. LEE N K, JANG J G AND LEE H K, Shrinkage characteristics of alkali-activated fly ash/slag paste and mortar at early ages, Cement and Concrete Composites, 2014, Vol. 53, pp 239-248.
19. KUMARAPPA D B, PEETHAMPARAN S AND NGAMI M, Autogenous shrinkage of alkali activated slag mortars: Basic mechanisms and mitigation methods, Cement and Concrete Research, 2018, Vol. 109, pp 1-9.
20. WALLAH S AND RANGAN B V, Low-calcium fly ash-based geopolymer concrete: long-term properties, Research Report GC 2, Faculty of Engineering, Curtin University of Technology, Perth, Australia, 2006.
21. GILBERT R I, Creep and shrinkage models for high strength concrete–proposals for inclusion in AS3600, Australian Journal of Structural Engineering, 2002, Vol. 4, No. 2, pp 95-106.
22. Committee BD-002 Standards Australia, Concrete Structures: Draft Australian Standard AS3600-200x, Standards Australia, 2005.
23. AMERICAN CONCRETE INSTITUTE COMMITTEE 209, 209.2R-08: Guide for Modeling and Calculating Shrinkage and Creep in Hardened Concrete, American Concrete Institute, Farmington Hills, MI, 2008, pp 44.
24. DEB P S, NATH P AND SARKER P K, The effects of ground granulated blast-furnace slag blending with fly ash and activator content on the workability and strength properties of geopolymer concrete cured at ambient temperature, Materials & Design, 2014, Vol. 62, pp 32-39.
25. FANG G, BAHRAMI H AND ZHANG M, Mechanisms of autogenous shrinkage of alkali-activated fly ash-slag pastes cured at ambient temperature within 24 h, Construction and Building Materials, 2018, Vol. 171, pp 377-387.
26. GAO X, YU Q L AND BROUWERS H J H, Reaction kinetics, gel character and strength of ambient temperature cured alkali activated slag–fly ash blends, Construction and Building Materials, 2015, Vol. 80, pp 105-115.

27. BAKHAREV T, SANJAYAN J G, AND CHENG Y-B, Effect of elevated temperature curing on properties of alkali-activated slag concrete, Cement and Concrete Research, 1999, Vol. 29, No. 10, pp 1619–1625.
28. COLLINS F AND SANJAYAN J G, Cracking tendency of alkali-activated slag concrete subjected to restrained shrinkage, Cement and Concrete Research, 2000, Vol. 30, No. 5, pp 791–798.
29. MA J AND DEHN F, Shrinkage and creep behavior of an alkali-activated slag concrete, Structural Concrete, 2017, Vol. 18, No. 5, pp 801-810.
30. AMERICAN SOCIETY FOR TESTING AND MATERIALS INTERNATIONAL, ASTM C618 – 17a, Standard Specification for Coal Fly Ash and Raw or Calcined Natural Pozzolan for Use in Concrete, West Conshohocken, PA, 2017.
31. AMERICAN SOCIETY FOR TESTING AND MATERIALS INTERNATIONAL, ASTM C989 / C989M-17, Standard Specification for Slag Cement for Use in Concrete and Mortars, ASTM International, West Conshohocken, PA, 2017.
32. AMERICAN SOCIETY FOR TESTING AND MATERIALS INTERNATIONAL, ASTM C33 / C33M–16e1, Standard Specification for Concrete Aggregates, West Conshohocken, PA, 2016.
33. AMERICAN SOCIETY FOR TESTING AND MATERIALS INTERNATIONAL, ASTM C494 / C494M – 17, Standard Specification for Chemical Admixtures for Concrete, West Conshohocken, PA, 2017.
34. AMERICAN SOCIETY FOR TESTING AND MATERIALS INTERNATIONAL, ASTM C157 / C157M-17, Standard Test Method for Length Change of Hardened Hydraulic-Cement Mortar and Concrete, West Conshohocken, PA. 2017.
35. DEIR E, GEBREGZIABIHER B S, AND PEETHAMPARAN S, Influence of starting material on the early age hydration kinetics, microstructure and composition of binding gel in alkali activated binder systems, Cement and Concrete Composites, 2014, Vol. 48, pp 108–117.
36. GEBREGZIABIHER B S, THOMAS R J, AND PEETHAMPARAN S, Very early age reaction kinetics and microstructural development in alkali-activated slag, Cement and Concrete Composites, 2015, Vol. 55, pp 91–102.
37. GEBREGZIABIHER B S, THOMAS R J, AND PEETHAMPARAN S, Temperature and activator effects on early-age reaction kinetics of alkali-activated slag binders, Construction and Building Materials, 2016, Vol. 113, pp 783–793.
38. ASTM C 490. Specification for apparatus for use in measurement of length change of hardened cement paste, mortar, and concrete. Annual Book of ASTM Standards, 04.01, 1988:265–268.
39. KAR A, RAY I, HALABE U B AND UNNIKRISHNAN A, Physicochemical and Microstructural Characterizations of Alkali-Activated Binder Systems, International Journal of Structural and Civil Engineering Research, 2016, Vol. 5, No. 2, pp 119-129.
40. KAR A, RAY I, HALABE U B AND UNNIKRISHNAN A, Nondestructive characterizations of alkali activated fly ash and/or slag concrete, European Scientific Journal, 2013, Vol.9 No.24, pp 52-74.
41. WANG G AND MA Y, Drying shrinkage of alkali-activated fly ash/slag blended system, Journal of Sustainable Cement-Based Materials, 2018, pp 1-11.

42. COLLINS F AND SANJAYAN J G, Effect of pore size distribution on drying shrinking of alkali-activated slag concrete, Cement and Concrete Research, 2000, Vol. 30, No. 9, pp 1401–1406.
43. PALACIOS M AND PUERTAS F, Effect of shrinkage-reducing admixtures on the properties of alkali-activated slag mortars and pastes, Cement and Concrete Research, 2007, Vol. 37, No. 5, pp 691–702.
44. LI J AND YAO Y, A study on creep and drying shrinkage of high performance concrete, Cement and Concrete Research, 2001, Vol. 31, No. 8, pp1203-1206.
45. YIP C K, LUKEY G C, PROVIS J L AND VAN DEVENTER J S J, Effect of calcium silicate sources on geopolymerisation, Cement and Concrete Research, 2008, Vol. 38, No. 4, pp 554–564.
46. YIP C K AND VAN DEVENTER J S J, Microanalysis of calcium silicate hydrate gel formed within a geopolymeric binder. Journal of Materials Science, 2003, Vol. 38, No. 18, pp 3851–3860.
47. YIP C K, LUKEY G C AND VAN DEVENTER J S J, The coexistence of geopolymeric gel and calcium silicate hydrate at the early stage of alkaline activation. Cement and Concrete Research, 2005, Vol. 35, No. 9, pp 1688–1697.
48. ALONSO S AND PALOMO A, Calorimetric study of alkaline activation of calcium hydroxide metakaolin solid mixtures, Cement and Concrete Research, 2001, Vol. 31, No. 1, pp 25–30.
49. ALONSO S AND PALOMO A, Alkaline activation of metakaolin and calcium hydroxide mixtures: influence of temperature, activator concentration and solids ratio, Materials Letters, 2001, Vol. 47, No. 1–2, pp 55–62.
50. DOMBROWSKI K, BUCHWALD A AND WEIL M, The influence of calcium content on the structure and thermal performance of fl y ash based geopolymers, Journal of Materials Science, 2007, Vol. 42, No. 9, pp 3033–3043.
51. FANG G, BAHRAMI H AND ZHANG M, Mechanisms of autogenous shrinkage of alkali-activated fly ash-slag pastes cured at ambient temperature within 24 h, Construction and Building Materials, 2018, Vol. 171, pp 377-387.
52. CHI M AND HUANG R, Binding mechanism and properties of alkali-activated fly ash/slag mortars, Construction and Building Materials, 2013, Vol. 40, pp 291-298.
53. MA Y, HU J, AND YE G, The pore structure and permeability of alkali activated fly ash, Fuel, 2013, Vol. 104, pp 771–780.
54. COLLINS F AND SANJAYAN J, Unsaturated capillary flow within alkali activated slag concrete, Journal of Materials in Civil Engineering, 2008, Vol. 20, No. 9, pp 565–570.
55. COLLINS F G AND SANJAYAN J G, Capillary shape: influence on water transport within unsaturated alkali activated slag concrete, Journal of Materials in Civil Engineering, 2010, Vol. 22, No. 3, pp 260–266.
56. THOMAS R J, LEZAMA D AND PEETHAMPARAN S, On drying shrinkage in alkali-activated concrete: Improving dimensional stability by aging or heat-curing, Cement and Concrete Research, 2017, Vol. 91, pp 13-23.